Proceedings of CONF-CIAP 2026 Symposium: International Conference on Atomic Magnetometer and Applications
DOI: 10.54254/2753-8818/2026.HZ29333

THESAN-ZOOM at High Redshift: Summary of Galaxy Formation, Dust, and Star Formation Histories

Yiduo Zhang

Harrow International School Hong Kong, Hong Kong, China
yiduozhang79@gmail.com

Abstract. This paper gives a summary of the THESAN-ZOOM project, a suite of high-resolution cosmological zoom-in simulations of galaxies in the high-redshift Universe. Building on the larger-volume THESAN simulations, THESAN-ZOOM achieves greater resolution within selected haloes, enabling the modelling of cold molecular gas, dust, radiation, and star-formation physics on the interstellar medium (ISM). Using a weighting scheme to map the zoom haloes onto a representative cosmological volume, the project generates synthetic galaxy populations for comparison with recent observations, particularly from the James Webb Space Telescope (JWST). This paper highlights results through key figures from the THESAN-ZOOM project, such as a multi-field view illustrating gas, dust, metals, and radiation densities, thermal phase diagrams, the galaxy stellar mass function, the rest-UV luminosity function, and the cosmic star-formation rate density. Together, these results demonstrate that THESAN-ZOOM provides a consistent framework for connecting the ISM to the evolution of galaxies across the epoch of reionisation.

Keywords: cosmological simulations, high-redshift galaxies, galaxy formation, dust and molecular gas, reionisation

1. Introduction

Numerical simulations have become key in understanding the origin and evolution of galaxies. They follow the processes of gravitational collapse, cooling, star formation, chemical enrichment, and radiation, all of which shape the structure of galaxies and their surrounding medium. Modern simulation codes, such as AREPO, allow gas flows to be treated with high fidelity, providing a platform for modelling cosmic structure formation [1].

The high-redshift Universe ($z \gtrsim 6$) has emerged as a central focus of both observational and theoretical efforts. This era corresponds to the epoch of reionisation, when the first generations of stars and galaxies ionized intergalactic hydrogen and initiated large-scale chemical enrichment. Galaxies formed during this period set the initial conditions for the growth of the universe. With the arrival of JWST, it is now possible to directly observe galaxies in this early era, revealing populations of luminous and massive systems. These discoveries have produced the need for simulations that can generate galaxy populations suitable for comparison with surveys [2].

© 2025 The Authors. This is an open access article distributed under the terms of the Creative Commons Attribution License 4.0 (https://creativecommons.org/licenses/by/4.0/).

DOI: 10.54254/2753-8818/2026.HZ29333

2. THESAN to THESAN-ZOOM

THESAN-1 is an example of a simulation aimed to address the need mentioned earlier. It followed a cosmological volume of 95.5 cMpc on a side with treatments of gas, star formation, stellar feedback, chemical enrichment, radiation, and dust. This allowed the project to model the global progress of reionisation, but the spatial and mass resolution were necessarily limited by the volume. As a result, the small-scale structure of ISM—particularly the cold, molecular, and dusty phases—was under-resolved. This restricted the ability to study star-formation histories [3].

To address this, the THESAN-ZOOM simulations were carried out. These consist of high-resolution re-simulations of individual haloes drawn from the parent THESAN volume. By 'zooming in' on selected haloes, the simulations achieve up to 64 times higher mass resolution while still embedding each target galaxy in its proper cosmological environment. This approach resolves the dense, cold gas clouds where molecular hydrogen forms, dust accumulates, and stars are born [1].

2.1. THESAN-ZOOM simulations

Table 1. Complete set of THESAN-ZOOM simulations. Reprinted from [1]

Simulation	Group number THESAN-DARK-1	M_{group} at $z = 3$ [$M_\odot$]	4x	8x	16x	4x noESF	4x noRlim	4x varEff	8x noESF	8x noRlim	8x varEff	8x UVB	8x lateUVB
m13.0	2	8.93×10^{12}	P	O	O	O	O	O	O	O	O	O	O
m12.6	39	4.07×10^{12}	P	O	O	O	O	O	O	O	O	O	O
m12.2	205	1.58×10^{12}	P	O	O	O	O	O	O	O	O	O	O
m11.9	578	7.70×10^{11}	P	O	O	P	O	O	O	O	O	O	O
m11.5	1163	3.28×10^{11}	P	O	O	P	O	O	O	O	O	O	O
m11.1	5760	1.40×10^{11}	P	P	O	P	P	P	O	O	O	O	O
m10.8	10304	5.93×10^{10}	P	P	O	P	O	O	O	O	O	O	O
m10.4	33206	2.53×10^{10}	P	P	O	P	P	P	P	P	P	P	P
m10.0	37591	1.07×10^{10}	P	P	O	O	O	O	O	O	O	P	P
m9.7	137030	4.58×10^{9}	P	P	P	P	P	P	P	P	P	P	P
m9.3	500531	1.95×10^{9}	P	P	P	O	O	O	O	O	O	P	P
m8.9	519761	8.29×10^{8}	P	P	P	O	O	O	O	O	O	P	P
m8.5	2274036	3.51×10^{8}	P	P	P	O	O	O	O	O	O	P	P
m8.2	5229300	1.52×10^{8}	P	P	P	O	O	O	O	O	O	P	P
Total		60	14	9	5	6	3	3	2	2	2	7	7

Table 1 provides the complete list of THESAN-ZOOM simulations. Each row lists a target halo, and the columns indicate which resolution levels and physical variations were performed.

The targets span over a wide range of halo masses, from ~109 M⊙ to ~1012 M⊙ at redshift 3. Each halo can be run at three resolution levels: 4×, 8×, and 16×, which is relative to the THESAN-1 run. All haloes have at least a 4× run, intermediate-mass haloes often include an 8× run, and the lowest-mass haloes are run at the 16× resolution.

DOI: 10.54254/2753-8818/2026.HZ29333

The right-hand side of Table 3 lists several physical variations. These are essentially controlled experiments with a certain aspect altered, such as delaying the activation of the UV background or modifying the star-formation efficiency. This strategy allows the project to separate the effects of numerical resolution from those of modelling choices [1].

2.2. Weighting scheme

Because zoom-in simulations cover only a small number of haloes, it can be difficult to compare their results with cosmological observations. To solve this, THESAN-ZOOM applies a weighting scheme that associates each zoom target with the abundance of haloes of similar mass in the parent volume. By weighting the contribution of each target according to the halo mass function, the ensemble of zooms can be combined to construct statistics such as stellar mass functions and luminosity functions, making the results directly comparable to survey data [1].

3. Results

3.1. Multi-field view at z = 3.2

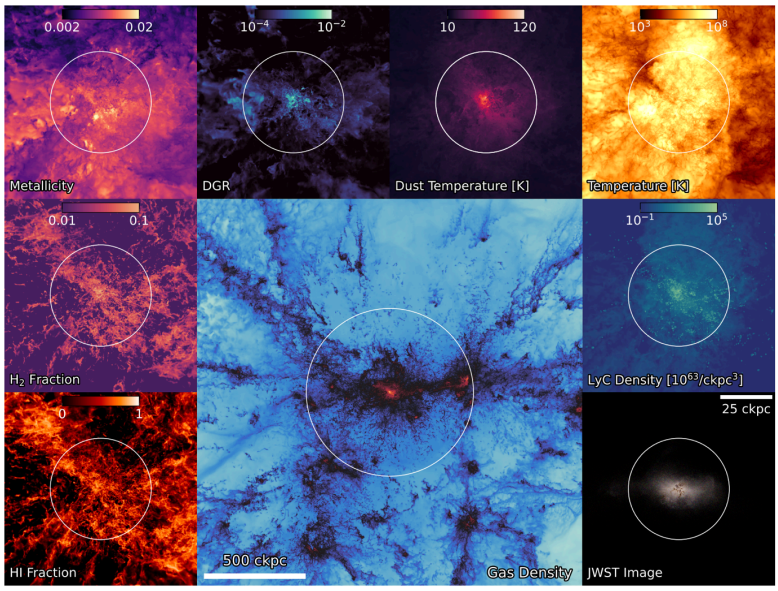

Figure 1. Multi-field overview of physical quantities predicted by THESAN-ZOOM. Reprinted from [1]

Figure 1 presents a qualitative, multi-field overview of a representative THESAN-ZOOM target (the m12.6_4x halo) at redshift $z = 2$. The central panel shows the gas-density field across a 2 comoving-Mpc region centered on the halo. Surrounding the central map are eight panels that display the same region by other fields, including neutral-hydrogen fraction, molecular-hydrogen fraction, gas-phase metallicity, dust-to-gas ratio, dust temperature, gas temperature, ionizing photon number density, and a mock JWST image [1].

This figure illustrates how different ISM components co-exist in space. For example, neutral hydrogen traces extended parts around the halo, whereas molecular hydrogen is mostly concentrated in dense, shielded clumps within the ISM.

This figure also demonstrates that THESAN-ZOOM attains the spatial and physical resolution necessary to resolve the multi-phase ISM at high redshift inside a proper cosmological environment.

DOI: 10.54254/2753-8818/2026.HZ29333

3.2. Stellar-to-halo mass relation

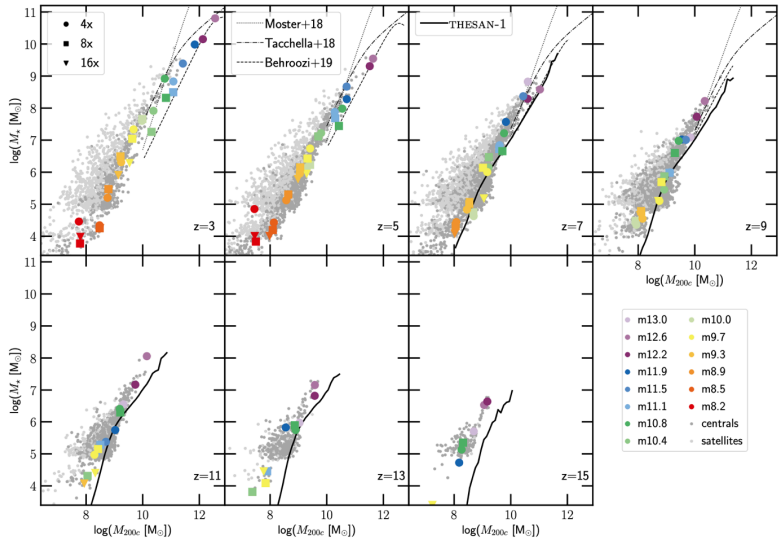

Figure 2. The stellar-to-halo mass relation. Reprinted from [1]

Figure 2 presents the stellar-to-halo mass relation for the THESAN-ZOOM simulations. The plot displays both central galaxies and satellites, with symbol color and shape indicating the simulation resolution used for each point. The reference curves from analytic models are also plotted, as well as the relation measured in the THESAN run [1].

Across the overlapping mass and redshift ranges, THESAN-ZOOM reproduces the shape of previously formulated relations. For example, for redshifts below ≈ 10, the simulated stellar masses lie close to the benchmarks. Therefore, the figure provides validation of the THESAN-ZOOM simulations, and, by showing centrals and satellites separately, the figure reflects the importance environmental effects that can displace points from the central relation.

3.3. Star formation rate versus stellar mass

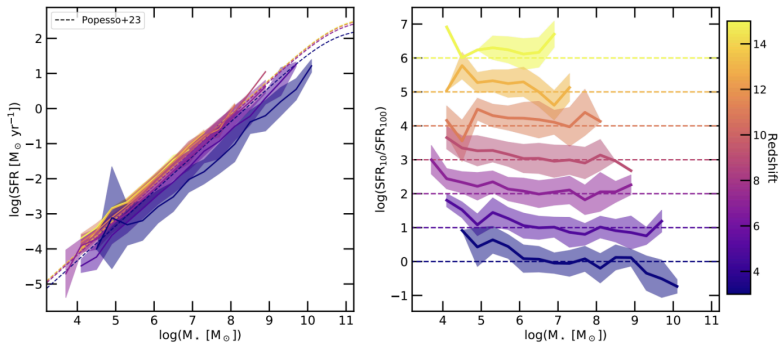

Figure 3. The star-formation rate to stellar mass relation for central galaxies. Reprinted from [1]

Figure 3 examines how star formation activity in THESAN-ZOOM galaxies scales with stellar mass across cosmic time. The figure is split into two panels.

The left panel plots the star formation rate (SFR) against stellar mass for central galaxies between redshifts $z = 3$ and $z = 15$. Each colored line shows the median relation at a given redshift, with

DOI: 10.54254/2753-8818/2026.HZ29333

shaded regions indicating the 1σ scatter. Overplotted dashed lines are inferred fits enabling direct comparison between the simulations and current data [4].

The right panel plots the SFR averaged over 10 Myr divided by the SFR averaged over 100 Myr as a function of stellar mass. Each redshift slice is offset vertically for clarity. Positive values correspond to galaxies whose star formation is rising, while negative values correspond to declining star formation activity [1].

The simulated relations show stronger redshift evolution than the observational fits. It is suggested that this difference may reflect observational incompleteness, particularly the difficulty of detecting faint, low-mass galaxies at high redshift. Nevertheless, the figure provides evidence that THESAN-ZOOM is broadly consistent with the observation data, confirming it produces a plausible star-forming main sequence across multiple redshifts.

3.4. Gas thermal phase diagrams

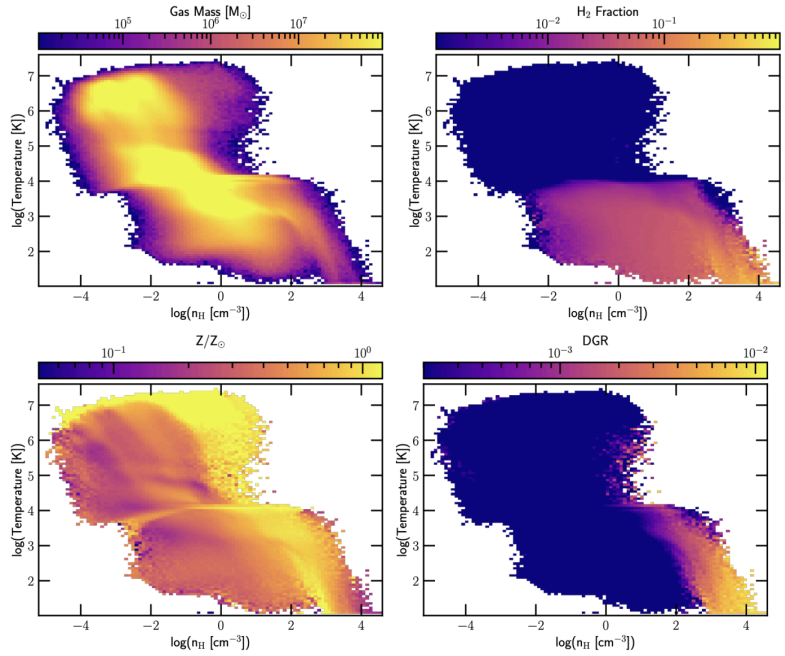

Figure 4. The temperature-density phase-space diagram at z= 3. Reprinted from [1]

Figure 4 presents thermal phase diagrams for the gas within the virial radius of a THESAN-ZOOM halo (the m12.6_4x target) at redshift z = 3. Each panel plots gas temperature against hydrogen number density, but with different weightings to highlight distinct physical factors. The top-left panel is mass-weighted, showing where most of the gas resides. The top-right panel is weighted by molecular hydrogen (H_2) fraction, the bottom-left by gas metallicity, and the bottom-right by dust-to-gas ratio [1].

Together, the four panels reveal the multiphase structure of the ISM. The mass-weighted panel shows gas distributed along two parts: a cold, dense component at high density, and a hot component occupying lower densities. The H_2-weighted panel demonstrates that molecular hydrogen is confined to the cold, dense area. The metallicity and dust-weighted panels trace similar regions, indicating that chemical enrichment is concentrated in the cold ISM.

A notable feature of the H_2 and dust distributions is that their important contribution comes not only from the densest clumps, but also from the broader cold, moderately dense area. The more

DOI: 10.54254/2753-8818/2026.HZ29333

extended cold areas surrounding the high-density regions collectively hold a much larger fraction of the total H_2 and dust mass. Consequently, these regions are central to fueling star formation.

3.5. Galaxy stellar mass function

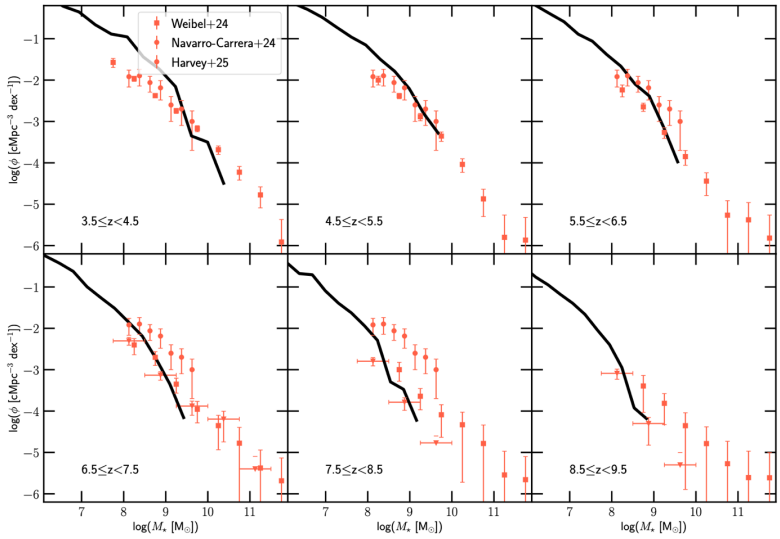

Figure 5. The galaxy stellar mass function. Reprinted from [1]

Figure 5 shows the galaxy stellar mass function (GSMF) derived from the THESAN-ZOOM simulations. The GSMF plots the number density of galaxies per stellar-mass bin against stellar mass with results presented at redshifts ranging from $z = 3.5$ to 9.5. The simulation results are volume-weighted using the halo-mass function so that the zoom sample can be compared directly with cosmological surveys. Observational data from JWST and earlier studies are also plotted for reference [1].

The simulated GSMFs demonstrate generally good agreement with observation. At $z \approx 5$–7, the GSMF from THESAN-ZOOM matches survey measurements closely across most of the accessible mass range. By $z \approx 4$, however, the simulation overpredicts the abundance of low-mass galaxies. At higher redshifts, the high-mass end becomes uncertain due to the limited volume of the simulations, which under samples the massive haloes.

Because THESAN-ZOOM consists of zoom-in simulations of selected haloes, the raw counts of galaxies cannot be a representative galaxy population. To correct for this, the authors implement a statistical weighting scheme which maps each simulated system back onto the cosmological halo mass function [5].

The procedure operates in several steps. First, all simulated snapshots are grouped into bins of halo mass and redshift. For each bin, the expected number of haloes is calculated using an analytic halo mass function. This gives the expected abundance of haloes that should exist in a reference volume. The number of simulated haloes in the bin is then counted. Each simulated halo in that bin is assigned a weight equal to the expected number divided by the simulated number. This weight specifies how many real haloes each zoom halo represents.

To derive the stellar mass function, the weighted snapshots are placed into stellar-mass bins. The weights of all galaxies within a given stellar-mass bin are summed and divided by the comoving volume corresponding to the chosen redshift range. This yields the galaxy stellar mass function, which is the number density of galaxies per stellar-mass interval.

DOI: 10.54254/2753-8818/2026.HZ29333

In general, the figure demonstrates that THESAN-ZOOM reproduces the observed galaxy stellar mass distribution over a wide redshift range, while also identifying specific redshift-dependent discrepancies.

3.6. UV luminosity function

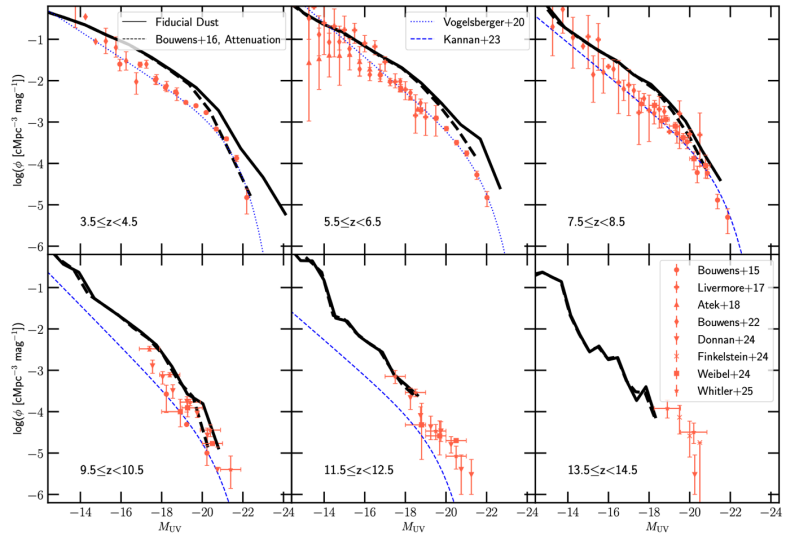

Figure 6. The UV luminosity function. Reprinted from [1]

Figure 6 presents the rest-frame ultraviolet luminosity function (UVLF) predicted by THESAN-ZOOM. The UVLF plots the number density of galaxies per unit magnitude against absolute UV magnitude. Simulation curves are shown both for the dust-free luminosities of galaxies and for the dust-attenuated luminosities computed using two different dust models: a fiducial prescription and another model tuned to high-redshift observational constraints. Observational measurements from JWST and HST surveys are plotted for comparison [1].

The figure shows that once dust attenuation is included, the simulated UVLFs reproduce observed galaxy counts well across a wide range of magnitudes and redshifts. The faint-end slope is well matched, reflecting the ability of the simulations to resolve low-mass galaxies. The bright end, however, is more sensitive: intrinsic luminosities overshoot the observations, while the attenuated curves bring the predictions into closer agreement.

4. Conclusion

The THESAN-ZOOM simulations open a new window on early galaxy formation by combining the parent THESAN runs with the resolution needed to model the multiphase ISM. By resolving molecular hydrogen, dust processes, and radiative transfer, they link the ISM directly to population statistics and observables from the epoch of reionisation.

The THESAN-ZOOM simulations reproduce the stellar-to-halo mass relation, recover a plausible and evolving star-forming main sequence, and match observed stellar mass and UV luminosity functions across most redshifts.

However, some limitations remain. The small number of zoom targets leads to uncertainty at the massive galaxies, while at $z \approx 4$ the abundance of low-mass galaxies is overpredicted. Dust treatment is the largest source of uncertainty: two different models bracket observed luminosity functions and SFRDs, showing how sensitive predictions are to dust assumptions.

DOI: 10.54254/2753-8818/2026.HZ29333

Overall, THESAN-ZOOM demonstrates that simulations can account for many high-redshift observables and provide physical explanations for JWST's discoveries. Future work can expand the zoom sample, refine feedback and dust modelling, and exploit joint JWST datasets to test predictions more rigorously.

References

[1] Kannan, R., Puchwein, E., Smith, A., Borrow, J., Garaldi, E., Keating, L., Vogelsberger, M., Zier, O., McClymont, W., Shen, X., Popović, F., Tacchella, S., Hernquist, L., & Springel, V. 2025. Introducing the THESAN-ZOOM project: radiation-hydrodynamic simulations of high-redshift galaxies with a multi-phase interstellar medium. arXiv preprint arXiv: 2502.20437.

[2] Trebitsch, M., Blaizot, J., and Rosdahl, J. 2015. Modeling small galaxies during the Epoch of Reionisation. arXiv preprint arXiv: 1510.06949.

[3] Kannan, R., Garaldi, E., Smith, A., Pakmor, R., Springel, V., Vogelsberger, M., and Hernquist, L. 2021. Introducing the THESAN project: radiation-magnetohydrodynamic simulations of the epoch of reionization. arXiv preprint arXiv: 2110.00584.

[4] Popesso, P., Concas, A., Cresci, G., Belli, S., Rodighiero, G., Inami, H., Dickinson, M., Ilbert, O., Pannella, M., & Elbaz, D. 2023. The main sequence of star-forming galaxies across cosmic times. Monthly Notices of the Royal Astronomical Society, 519(1), 1526–1541. https: //doi.org/10.1093/mnras/stac3214.

[5] Ma, X., Hopkins, P. F., Garrison-Kimmel, S., Faucher-Giguère, C.-A., Quataert, E., Boylan-Kolchin, M., Hayward, C. C., Feldmann, R., & Kereš, D. 2020. Simulating galaxies in the reionization era with FIRE-2: galaxy scaling relations, stellar mass functions, and luminosity functions. Monthly Notices of the Royal Astronomical Society, 491(1), 1–19. https: //doi.org/10.1093/mnras/stz3035.